Journal of Structural Geology 32 (2010) 2–14

Contents lists available at ScienceDirect

Journal of Structural Geology

journal homepage: www.elsevier.com/locate/jsg

Comparison of petrofabrics with composite magnetic fabrics of S–C mylonite in paramagnetic granite

Takaaki Ono [a,1], Yukinobu Hosomi [a,2], Hiroyoshi Arai [b], Hideo Takagi [b,*]

[a] Department of Earth Sciences, Graduate School of Science and Engineering, Waseda University, 1-6-1 Nishiwaseda, Shinjuku-ku, Tokyo 169-8050, Japan
[b] Department of Earth Sciences, Faculty of Education and Integrated Arts and Sciences, Waseda University, 1-6-1 Nishiwaseda, Shinjuku-ku, Tokyo 169-8050, Japan

ARTICLE INFO

Article history:
Received 30 January 2008
Received in revised form
17 April 2009
Accepted 18 April 2009
Available online 3 May 2009

Keywords:
AMS
Shear zone
Composite planar fabric
Paramagnetic granite
S–C mylonite

ABSTRACT

An anisotropy of magnetic susceptibility (AMS) analysis was conducted for a typical S–C mylonite in a small-scale ductile shear zone derived from Late Cretaceous magnetite- free granite in the Ryoke Belt, Teshima Island, southwest Japan. In such mylonites, paramagnetic minerals such as biotite and hornblende, which define foliations, are assumed to control the AMS. Accordingly, we attempted to measure the orientations of both minerals to correlate the S–C–C′ fabric to the AMS using techniques of microscopic and back-scattered electron (BSE) image analyses. A measured magnetic fabric of the S–C mylonite that is expressed by a K_{min} normal plane (K_{max}–K_{int} plane) approximated S foliation, K_{max} orientation coincided well with the orientations of mean resultant vectors for long axes of biotite and minor hornblende, whereas K_{max} did not coincide well with those of the mean resultant vectors for long axes of the brighter domain (aggregates of biotite and minor hornblende) from the binary BSE image. These results show that the magnetic fabric fairly reflects the shape preferred orientation of individual grains of paramagnetic monoclinic minerals, especially biotite, which forms the S–C–C′ fabric.

1. Introduction

The anisotropy of magnetic susceptibility (AMS) is affected by the sum of the contributions of each magnetic (diamagnetic, paramagnetic, ferromagnetic) mineral type in proportion to its volume fraction, mean susceptibilities and mineral intrinsic AMS (e.g. Borradaile and Jackson, 2004). AMS is a symmetrical second-order tensor (K_{ij}), which relates the intensity of the applied field (H_j) to the acquired magnetization (M_i) of a mineral through the equation: $M_i = K_{ij}H_j$ (Hrouda, 1982). The tensor is geometrically expressed by an ellipsoid specified by its principal eigenvalues (susceptibility magnitudes) and eigenvectors (their orientations), $K_{max} \geq K_{int} \geq K_{min}$ (e.g. Tarling and Hrouda, 1993). In the case of deformed magnetite-free granitic rocks, paramagnetic Fe-bearing silicates, which define foliations, are responsible for AMS (e.g. Rochette, 1987; Archanjo et al., 1994). For instance, when single preferred orientation fabrics exist in a rock, AMS is a powerful tool to investigate petrofabric, because its principal axis (K_{max}, K_{int}, K_{min}) often corresponds with the principal axis (X, Y, Z) of finite strain (e.g. Borradaile and Henry, 1997). In contrast, when multiple mineral orientations are present in a rock, a measured magnetic fabric will reflect a composite of these orientation fabrics (Borradaile and Tarling, 1981). Such composite magnetic fabrics do not correspond to finite strain. A situation of importance to structural geology where this issue might arise is in the use of AMS to infer deformation in an S–C mylonite. For example, Tomezzoli et al. (2003) reported that the magnetic foliation, defined as the plane normal to K_{min}, of S–C mylonite departs from the orientations of the S-plane. The magnetic foliation of deformed rocks with S–C structure can show an intermediate orientation between the S- and the C-planes reflecting the additive effect of two planar structures (Aranguren et al., 1996).

The main aim of this study is to use a single sample across an S–C mylonitic shear zone to investigate the relationships of the AMS geometry with rock fabric geometry. The advantage of this approach is that a detailed spatial comparison from the perimeter to a shear zone center is achieved. For this analysis, the AMS is characterized by the content of paramagnetic Fe-bearing minerals, the mineral shape-fabric by optical inspection, and the mineral-aggregate shape fabric by back-scatter electron (BSE) image analysis.

2. Geological setting

The S–C mylonite sample is from magnetite-free, biotite-hornblende granite in the Teshima Island, Seto Inland Sea, southwest

* Corresponding author.
E-mail address: hideo@waseda.jp (H. Takagi).
[1] Present address: Daiwa Institute of Research, Ltd., Tokyo 135-8460, Japan.
[2] Present address: Mainichi Broadcasting System, Inc., Osaka 530-8304, Japan.

0191-8141/$ – see front matter © 2009 Elsevier Ltd. All rights reserved.
doi:10.1016/j.jsg.2009.04.009

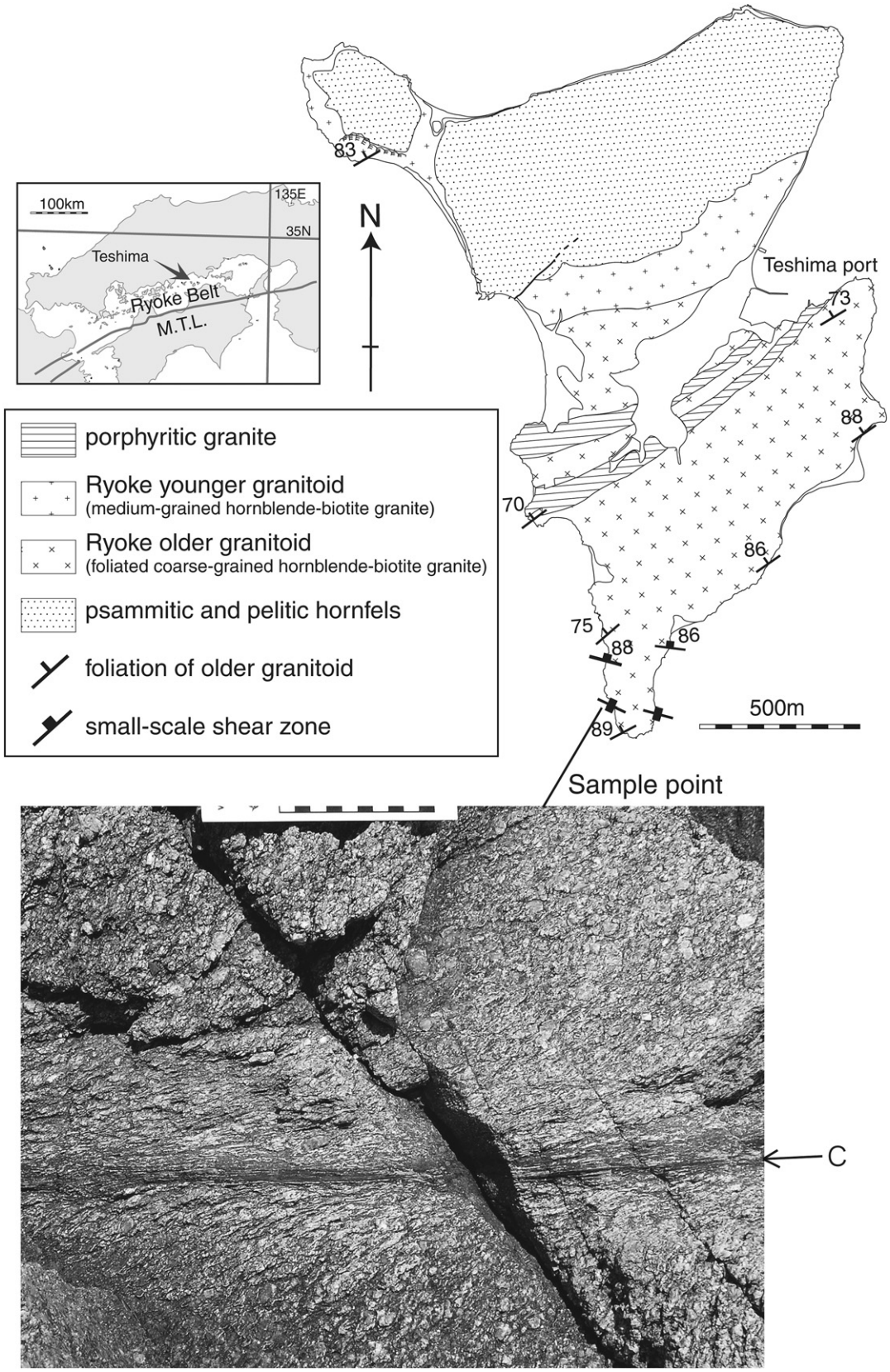

Fig. 1. Geological map of Teshima Island, Seto Inland Sea, SW Japan. The shear zone sample point is shown in the bottom picture in which the scale is in centimeters. C, shear zone center.

Japan (34°22′60″ N, 133°39′55″ E). This island is located in the Ryoke Belt, which is composed of Late Cretaceous foliated older granite and non-foliated younger granite, and metamorphic rocks, which occur as a roof pendant on the granitoid (Fig. 1). The granitic rocks in the Ryoke belt are low-susceptibility, ilmenite-series granitoid (Ishihara, 1981). Weakly mylonitized coarse-grained hornblende-biotite older granite, which strikes approximately ENE–WSW and dips subvertically, is widely exposed in the south of the island (Arita, 1988). Within the older granite, about 25 small-scale dextral ductile shear zones with a thickness ranging from several centimeters to a few meters are observed around the southernmost coastal area of the island. The shear zones have S–C–C′ fabrics and shear zone orientation strike WNW with subvertical dip, that crosscuts an older mylonitic foliation striking ENE.

The analyzed S–C mylonite sample (Fig. 2) was collected as a half side of the cross section of an entire shear zone that strikes N59°W with vertical dip and is about 50° oblique to the older foliation in the surrounding host older granite (N62–74°E, 90°). The S-foliation (Fig. 2) is defined by a shape fabric of biotite, quartz aggregate and elongated porphyroclasts. A sigmoidal deflection of the S foliation varying in angles with respect to the shear zone center (C-plane) from 60° to 10° gives a dextral shear sense (Fig. 2). This shear zone can be divided into three by grade of mylonitization; strongly, moderately and weakly mylonitized zones (SMZ, MMZ, WMZ). The distance from the shear zone center for each zone is 0–6 cm for SMZ, 6–14 cm for MMZ and over 14 cm for WMZ. Shear bands (C′), which are inclined at 5–25° clockwise to the C-plane dominate at the MMZ to SMZ near the shear zone center (Fig. 3). This oblique angle range between C′ and C is the as same as that described by Michibayashi and Murakami (2007).

3. Sample preparation and analytical methods

The sample analyzed covers about 35 cm from the shear zone center where the C plane and stretching lineation can be observed (Fig. 2). The angle between the C plane and the cut plane is about

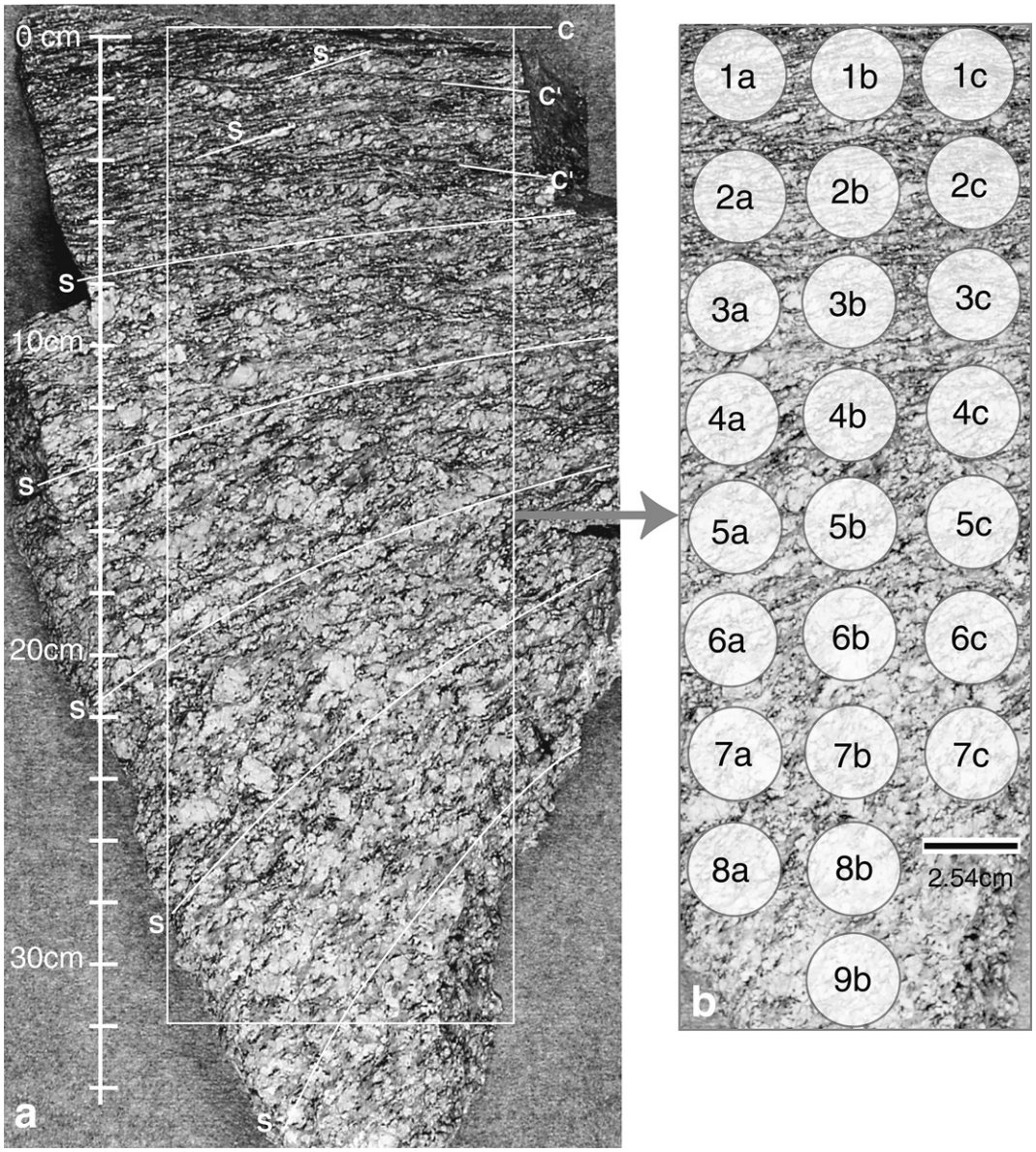

Fig. 2. (a) The analyzed S–C(-C′) mylonite cut subparallel to the *XZ* plane. Sigmoidal deflection of the S foliation (white lines) gives a dextral shear sense. (b) Locations and labels of core and thin section samples.

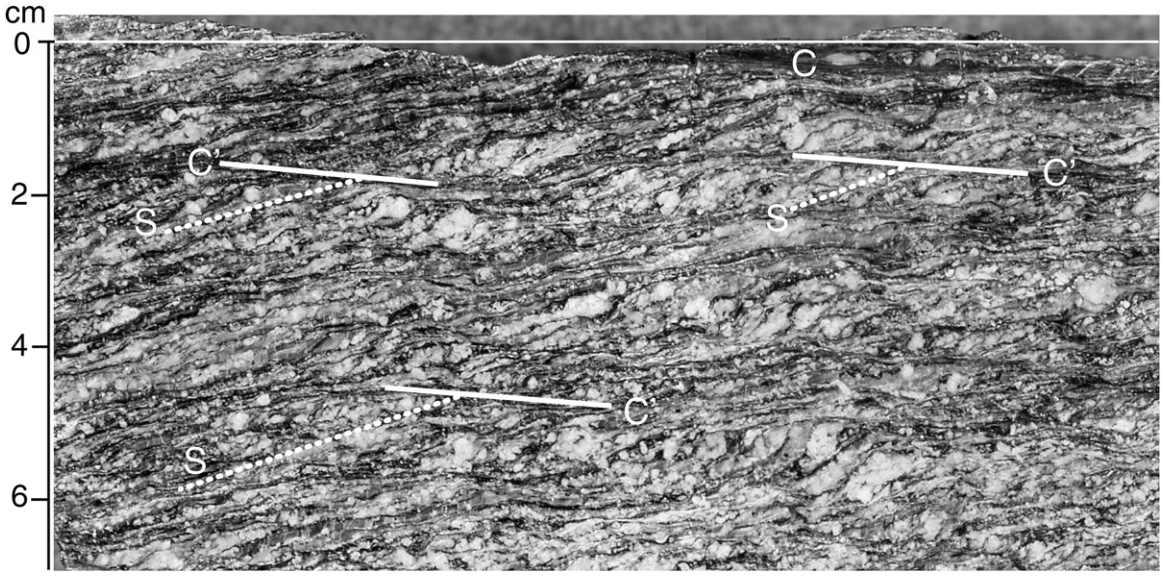

Fig. 3. Close-up near the shear zone center showing S–C–C′ fabric. Scale corresponds to Fig. 2 and this picture is located at the top of Fig. 2.

75°, and thus, the polished surface (Fig. 2a) is not exactly the *XZ* plane. When we estimated shear strain γ, using $\gamma = 2/\tan 2\theta_o$ after Ramsay and Graham (1970), we corrected the measured apparent angle θ_o into the real angle θ_r as a formula, $\tan\theta_r = \cos 15^\circ \tan\theta_o$ where 15° is the angle between the *XZ* plane and the sample plane. However, the difference between θ_o and θ_r is within the measuring error (for example, $\theta_r = 45^\circ$ in the case where $\theta_o = 46^\circ$ for sample 8a). Therefore, no correction for the 15° obliquity above is included in the analysis. Cylindrical core samples were drilled into the direction subparallel (about 15°) to the *Y*-axis normal to the polished *XZ* plane (Fig. 2b). Twenty-four cylindrical oriented specimens (diameter = 2.54 cm) were extracted by drilling with a non-magnetic diamond drill bit. AMS measurements were performed on 2.54 cm (diameter) × 2.2 cm (length) core samples, cut from the oriented specimens using a diamond tipped non-magnetic saw blade. Thin sections subparallel to the *XZ* plane were also prepared from the oriented core samples. Little asymmetric fabric was detected in the *YZ* thin sections, therefore the mylonite was characterized as having monoclinic fabric symmetry. Accordingly, we measured the fabrics and content of mafic minerals for each cylindrical sample in only the *XZ* section.

3.1. Microscopic analyses

To compare petrofabrics with the AMS data, foliations defined by biotite and hornblende were analyzed. All individual grains of biotite and hornblende within the same 16 × 16 mm sample areas as the BSE images (samples 3a to 8a) were analyzed, if grains of these minerals could be resolved microscopically. The minimum grain size measured is about 20 μm using 10 (eyepiece) × 20 (objective) lenses. The length of long axis *a* and short axes *b*, the angle θ between the long axis of biotite (+hornblende) and the C plane, and the modal percentage of each mineral were measured for samples 3a to 8a microscopically by point-counting (Fig. 4). The grain orientation (θ) data are shown as rose diagrams (Fig. 4). The grain size *d* of each mineral is defined as $d = (ab)^{1/2}$, and the grain area *s*, as $s = \pi ab/4$ to approximate an ellipse. The biotite (+hornblende) grains were divided into two groups: one with orientation subparallel to S, and the other subparallel to C′. The area *s* of the grains in both groups was compared (Fig. 4). The mean grain areas subparallel to C′ are a little smaller than or nearly the same as those parallel to S.

The mean vectors θ_m of long axis orientations for the biotite + hornblende in each sample were statistically calculated. θ_m and θ_o correspond to each other within a difference of 2°(Fig. 4), which is within the measuring error for θ_o from the sample. The shape preferred orientation (SPO) of biotite does not show random or symmetric unimodal distribution but is polymodal in the MMZ and broad in the WMZ (Fig. 4). To clarify the nature of the distribution of the SPO, we employed Watson's test for circular uniformity and von Mises distribution (Stephens, 1970; Jammalamadaka and SenGupta, 2001). The von Mises distribution is a symmetric unimordal distribution on a circle, which is analogous to the normal (Gaussian) distribution in linear data. Using Watson's test for circular uniformity, all the orientation data θ_m give circular uniformity at the significance level of 5%, which implies that all the SPO are statistically relevant, not random. The results of Watson's test for the von Mises distribution show all the samples excepting no. 8a do not follow the von Mises distribution at the significant level of 5%. This means that the SPOs of samples 3a to 7a are not unimodal. Several identified peaks must indicate the development of the composite planar fabrics such as S, C, and C′ in the shear zone as mentioned later.

3.2. BSE image analyses

Back-scattered electron (BSE) images (Fig. 5) were collected from polished thin sections, 1a to 8a, using an EPMA (JXA-8900) at the Department of Earth Sciences, Waseda University, to determine the fabrics of biotite and hornblende. Excepting biotite (partly altered chlorite) and hornblende, the BSE bright minerals such as opaque minerals are negligible (less than 0.1% in mode). The BSE images of biotite and hornblende are fairly bright reflecting a high mean atomic number, therefore biotite and hornblende were extracted together as binary images of the BSE (Fig. 5). The imaging area is 4 mm × 4 mm for 800 × 800 pixels (i.e. a resolution of 5 μm/pixel), and 16 areas are combined as a BSE image (Fig. 5).

The characteristics of the BSE image analysis are that (1) each domain is composed of an individual grain or an aggregate of grains of biotite and hornblende, (2) biotite and hornblende may be measured as very fine-grained domains especially in the

Sample	Orientation frequency of Bt (+Hb) with respect to S_o and C'	SPO of biotite (+hornblende)	Mode % Bt and Hb	Mean grain size (μm) Qz	Mean grain size (μm) Bt (+Hb)	Mean area (μm²) of Bt (+Hb) grains divided by orientation
SMZ 1a		θ_o =15° (γ not determined)	(Bt+Hb:8.4%)	66.9 52.0		
SMZ 2a		θ_o =13° (γ not determined)	(Bt+Hb:7.5%)	66.6 77.5		
MMZ 3a	$f_{So(2\sim22°)}$: 25.6% $f_{C'}$: 20.4%	θ_o =12° (γ = 4.7) θ_m=12.8° $\bar{R}$=0.52	Bt: 6.5% Hb: 0.7%	104.0 63.2	42.0 31.6	// C': 1535 // S: 1496
MMZ 4a	$f_{So(6\sim26°)}$: 24.4% $f_{C'}$: 14.8%	θ_o =16° (γ =3.4) θ_m =16.5° $\bar{R}$ =0.54	Bt: 6.4% Hb: 0.1%	100.2 91.7	45.3 31.6	// C': 1488 // S: 1689
WMZ 5a	$f_{So(12\sim32°)}$: 23.2% $f_{C'}$: 11.7%	θ_o =22° (γ =2.2) θ_m =24.1° $\bar{R}$ =0.52	Bt: 4.8% Hb: 0.1%	146.7 109.5	56.5 31.6	// C': 2026 // S: 2879
WMZ 6a	$f_{So(18\sim38°)}$: 21.0% $f_{C'}$: 11.0%	θ_o = 28° θ_m = 29.8° $\bar{R}$ = 0.48	Bt: 4.4% Hb: 0.1%	168.9 91.7	59.7 31.6	// C': 2784 // S: 2732
WMZ 7a	$f_{So(29\sim49°)}$: 16.5% $f_{C'}$: 10.3%	θ_o = 39° θ_m = 37.0° $\bar{R}$ = 0.41	Bt: 3.9% Hb: 0.4%	176.5 183.3	55.4 31.6	// C': 2640 // S: 3168
WMZ 8a	$f_{So(36\sim56°)}$: 26.5% $f_{C'}$: 7.2%	θ_o = 46° θ_m = 43.7° $\bar{R}$ = 0.50	Bt: 5.1% Hb:<0.1%	194.8 183.3	94.8 77.4	// C': 7943 // S: 8552
				Upper: geometric mean Lower: mode		Geometric mean

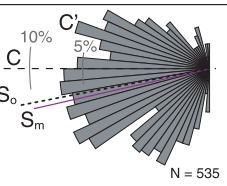

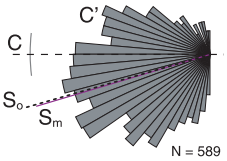

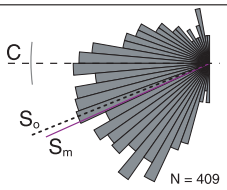

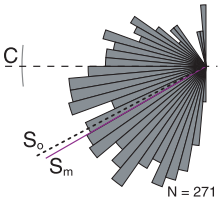

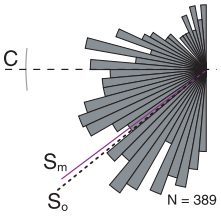

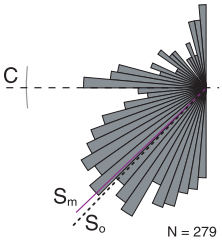

counted angular intrerval (20°) of orientation frequency
f_{So}: ±10° with respect to S_o
$f_{C'}$: –5°~–25° with respect to C
S_o: observed foliation
S_m: measured average orientation
$\bar{R}$: Mean resultant length

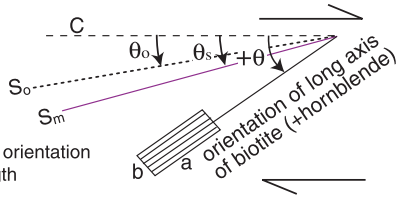

Fig. 4. Fabric data for mafic minerals and recrystallized quartz of S–C mylonite. Rose diagrams indicate the orientation of biotite (+hornblende) grains. The radius r of the rose diagrams is presented as the square root of the relative frequency. f_{So}, orientation frequency of biotite (+hornblende) subparallel (±10°) to the observed S plane (S_o, broken line), $f_{C'}$, orientation frequency of biotite (+hornblende) at an angle interval of −5° to −25° (observed angle interval of C′ on the sample surface and under the microscope) with respect to the C plane. The modal % of biotite (+hornblende), geometric mean and mode of grain size ($d = (ab)^{1/2}$) of recrystallized quartz and of biotite (+hornblende), and calculated mean grain area ($s = \pi ab/4$) for biotite (+hornblende) orientations measured in division of θ_{So} and $\theta_{C'}$ are shown.

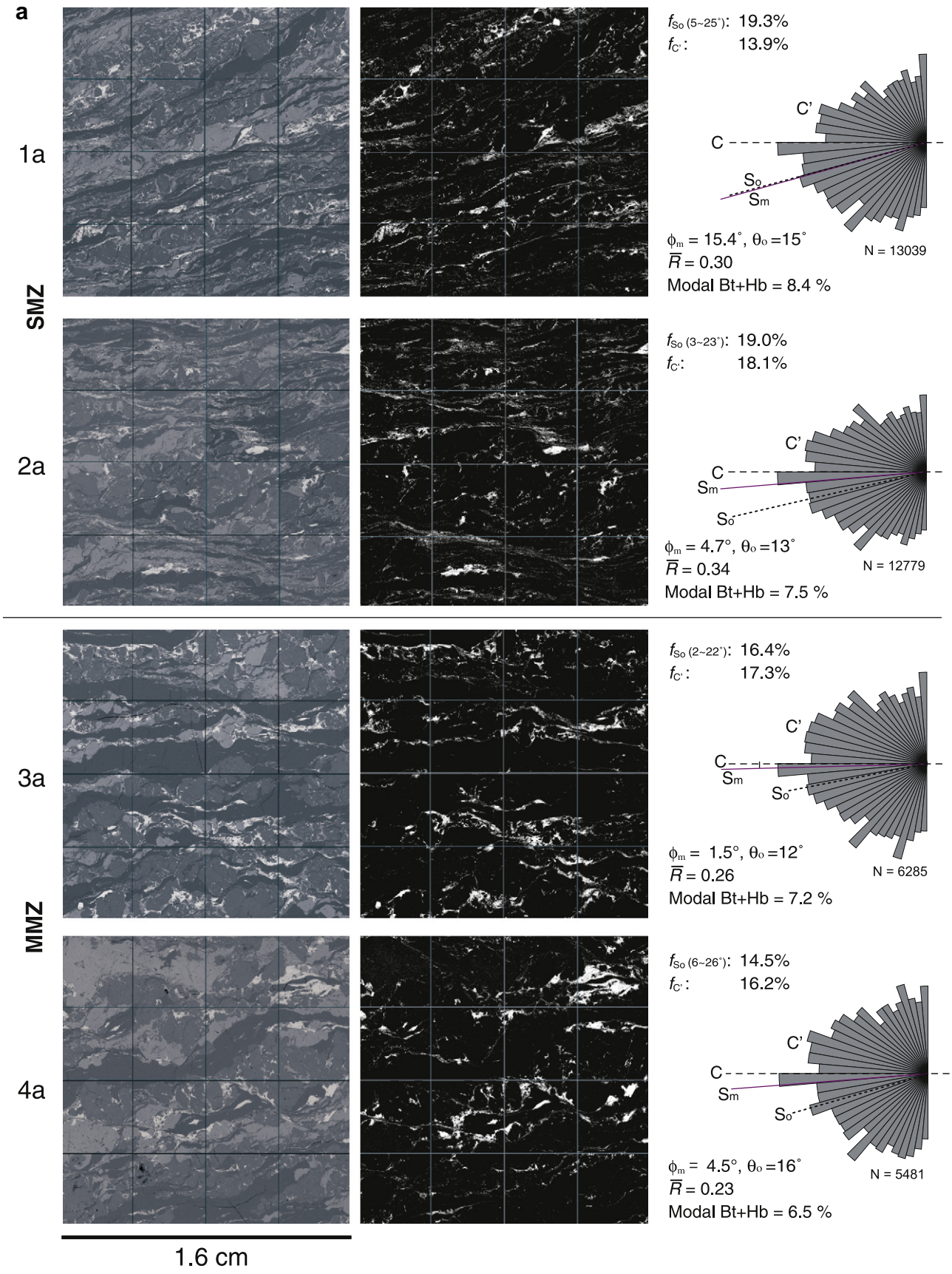

Fig. 5. Orientation data as rose diagrams from back-scattered electron (BSE) images of polished thin sections 1a to 8a (left pictures) and of binary images of BSE extracted biotite and minor hornblende (right pictures). Using the binary BSE images, the area of each bright domain and the angle between the long axis of approximated ellipse for each domain and C were measured by Scion (NIH) Image. f_{So}, orientation frequency of the bright domain subparallel ($\pm10^\circ$) to the observed S plane (S_o), $f_{C'}$, orientation frequency of the bright domain at an angle interval of $-5^\circ$to -25° with respect to the C plane. ϕ_m: The mean measured angle of orientation for bright domains with respect to C. The modal % of the brighter domain is also calculated.

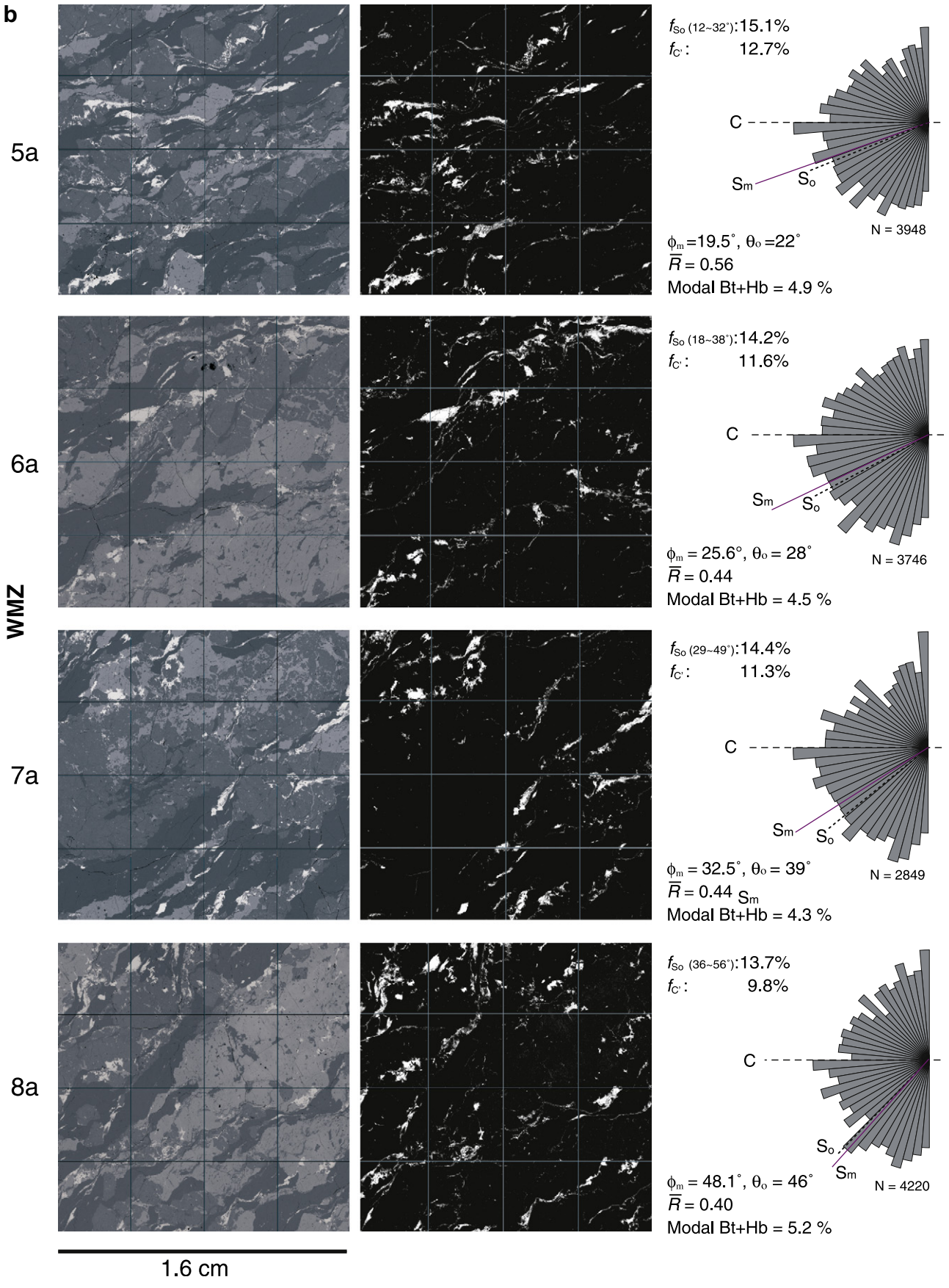

Fig. 5. (*continued*).

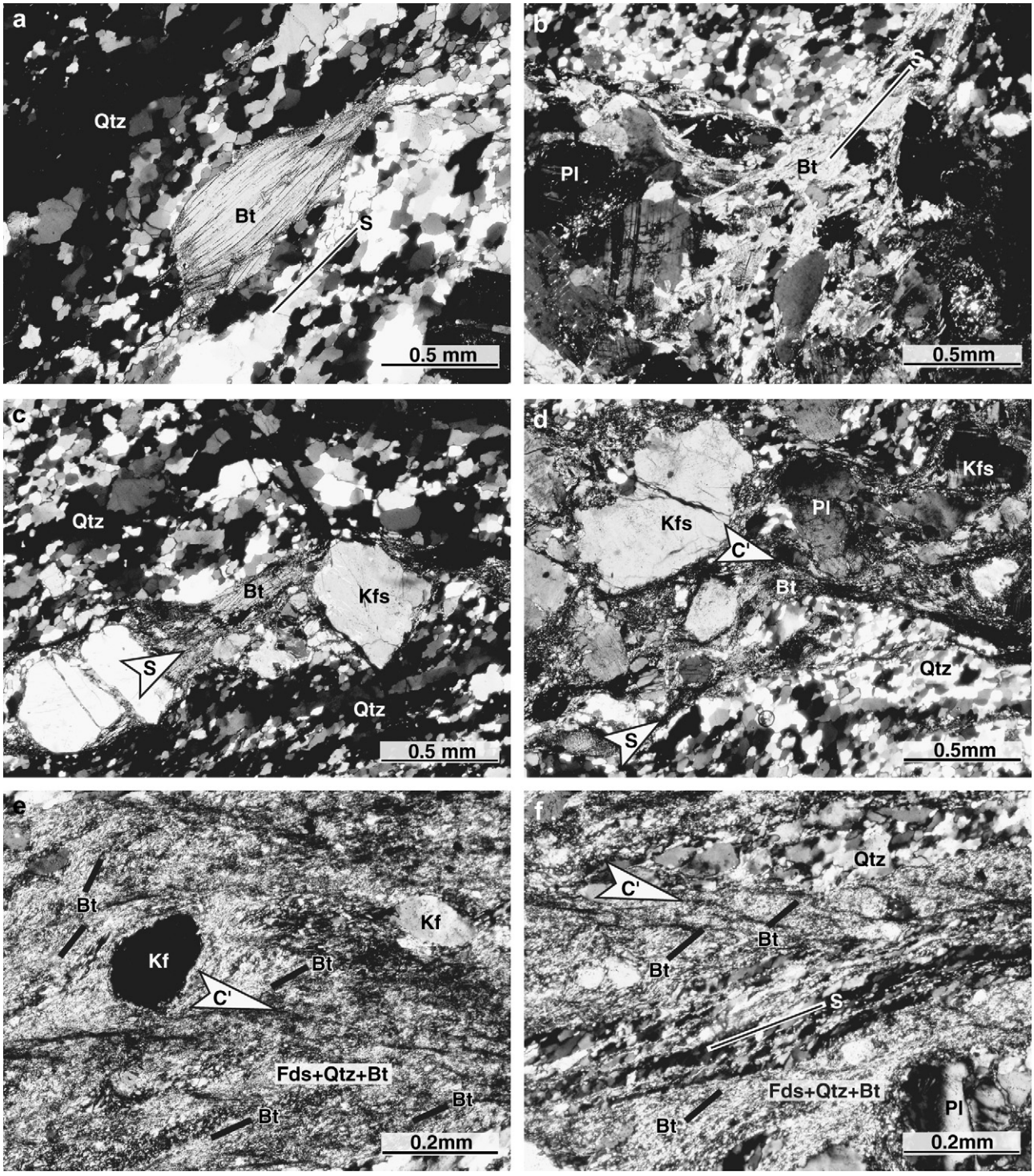

Fig. 6. Photomicrographs of the analyzed S–C mylonite (crossed polarized). (a) Coarse-grained biotite flakes constituting S foliation in WMZ (sample 8b). (b) Assembly of secondary biotites constituting S foliation in WMZ (samples 5a, b, c). (c) Biotite flakes constituting S in MMZ (sample 4b). (d) Tails of biotite constituting a major shear band (C′) in MMZ (sample 3b). (e) Minor shear bands (C′) in fine-grained aggregate of feldspar–quartz–biotite in SMZ (sample 2b). The orientation of fine-gained biotite flakes (black bars) is commonly clockwise oblique to the S. (f) Interlayering recrystallized quartz aggregate and very fine-grained feldspar–quartz–biotite aggregate in SMZ with C′ shear bands (sample 1b). Qtz, quartz; Fds, feldspar; Pl, plagioclase; Kfs, K-feldspar; Bt, biotite.

SMZ, and (3) the characteristics of the domains are easily quantified by using Adobe Photoshop® and Scion (NIH) Image software.

In the same way as the SPO from the optical microscope, all the SPOs from BSE images show neither a uniform distribution from the Watson test nor a circular distribution from the von Mises test at the significance level of 5%. The angle between the mean vector of the measured domains and the C plane is labeled as ϕ_m. The percentage area of the BSE bright minerals (biotite and hornblende) was also calculated as modal data. The labels of grouping criteria for orientations assigned to S and C′ are in addition to those for microscopic analyses as mentioned above (see Fig. 5a,b).

Table 1
AMS-orientation data and anisotropy parameters after Jelinek (1981)

sample	K_{mean} ($\times 10^{-6}$ SI)	Pj	T	K_{max}.Dec	K_{max}.Inc	K_{int}.Dec	K_{int}.Inc	K_{max}.Dec	K_{max}.Inc
1a	112.6 ± 1.3	1.119 ± 0.003	0.551 ± 0.047	65 ± 0.5	6.4 ± 0.8	176 ± 2.3	73 ± 0.0	333 ± 0.7	16 ± 0.4
2a	123.0 ± 3.2	1.100 ± 0.002	0.488 ± 0.024	72 ± 1.6	5.5 ± 1.1	185 ± 5.6	76 ± 0.5	341 ± 1.5	13 ± 0.0
3a	116.2 ± 2.1	1.070 ± 0.001	0.470 ± 0.011	258 ± 0.0	2.3 ± 1.1	163 ± 2.9	70 ± 0.4	349 ± 0.7	20 ± 0.0
4a	104.7 ± 0.4	1.066 ± 0.001	0.390 ± 0.010	254 ± 1.9	5.5 ± 0.9	149 ± 3.8	69 ± 0.5	346 ± 1.5	21 ± 0.4
5a	145.2 ± 1.3	1.082 ± 0.000	0.373 ± 0.015	244 ± 0.4	2.8 ± 0.4	145 ± 0.4	71 ± 0.4	334 ± 0.8	19 ± 0.4
6a	144.0 ± 2.2	1.073 ± 0.001	0.509 ± 0.018	240 ± 1.6	1.5 ± 0.5	150 ± 5.5	69 ± 0.4	330 ± 0.8	21 ± 0.4
7a	146.9 ± 0.4	1.079 ± 0.001	0.486 ± 0.034	57 ± 1.3	2.3 ± 1.1	152 ± 3.3	63 ± 0.4	326 ± 1.0	27 ± 0.4
8a	173.8 ± 0.5	1.091 ± 0.000	0.435 ± 0.019	45 ± 0.5	3.0 ± 1.6	142 ± 4.0	67 ± 0.5	313 ± 0.4	23 ± 0.4
1b	101.0 ± 0.3	1.105 ± 0.001	0.505 ± 0.024	75 ± 0.0	6.3 ± 1.3	187 ± 4.4	74 ± 0.5	344 ± 0.5	15 ± 0.0
2b	121.8 ± 2.2	1.097 ± 0.003	0.485 ± 0.009	78 ± 1.2	0.5 ± 0.5	169 ± 2.9	74 ± 0.0	348 ± 1.3	16 ± 0.0
3b	133.1 ± 0.4	1.165 ± 0.000	−0.087 ± 0.004	266 ± 0.0	0.0 ± 0.0	176 ± 0.7	23 ± 0.0	356 ± 1.3	67 ± 0.0
4b	108.6 ± 2.1	1.058 ± 0.002	0.448 ± 0.008	250 ± 0.4	1.8 ± 1.1	154 ± 4.3	75 ± 0.4	341 ± 0.5	15 ± 0.4
5b	124.1 ± 2.9	1.080 ± 0.002	0.405 ± 0.008	241 ± 0.5	3.5 ± 0.5	141 ± 0.7	72 ± 0.5	332 ± 0.8	18 ± 0.0
6b	122.0 ± 1.7	1.080 ± 0.001	0.444 ± 0.031	63 ± 0.9	2.3 ± 1.3	160 ± 4.7	72 ± 0.4	332 ± 0.4	18 ± 0.4
7b	169.2 ± 1.0	1.087 ± 0.000	0.485 ± 0.042	52 ± 0.4	3.3 ± 0.4	149 ± 1.4	67 ± 0.5	321 ± 0.5	23 ± 0.4
8b	161.8 ± 2.4	1.091 ± 0.002	0.321 ± 0.027	229 ± 1.7	0.3 ± 0.4	138 ± 2.1	65 ± 0.4	319 ± 1.3	25 ± 0.4
9b	144.8 ± 2.7	1.092 ± 0.002	0.309 ± 0.031	53 ± 0.5	2.5 ± 0.5	147 ± 1.2	65 ± 0.5	322 ± 0.5	25 ± 0.0
1c	105.5 ± 0.7	1.107 ± 0.001	0.493 ± 0.011	69 ± 0.9	5.5 ± 1.1	177 ± 3.8	73 ± 0.4	337 ± 0.4	16 ± 0.4
2c	116.9 ± 1.6	1.099 ± 0.002	0.493 ± 0.046	71 ± 1.4	3.0 ± 11	173 ± 5.5	75 ± 0.5	341 ± 1.1	15 ± 0.6
3c	109.4 ± 1.5	1.066 ± 0.001	0.519 ± 0.017	79 ± 0.8	6.0 ± 1.2	192 ± 4.5	75 ± 0.7	348 ± 0.4	14 ± 0.4
4c	98.8 ± 3.4	1.057 ± 0.002	0.372 ± 0.015	253 ± 0.0	2.0 ± 0.7	156 ± 2.9	73 ± 0.4	344 ± 0.5	17 ± 0.5
5c	127.3 ± 1.3	1.058 ± 0.001	0.470 ± 0.022	234 ± 1.8	4.0 ± 2.5	134 ± 7.1	68 ± 0.0	326 ± 1.1	22 ± 0.5
6c	146.7 ± 2.3	1.083 ± 0.001	0.487 ± 0.033	242 ± 0.8	0.8 ± 0.8	151 ± 3.3	71 ± 0.0	333 ± 1.1	19 ± 0.0
7c	144.4 ± 2.9	1.085 ± 0.001	0.304 ± 0.048	229 ± 0.4	5.5 ± 0.9	124 ± 2.1	70 ± 0.4	321 ± 0.5	20 ± 0.4

4. Variation of fabrics across the shear zone

4.1. Weakly mylonitized zone (WMZ): characteristics of samples 9 to 5

The mylonitic foliation of the protolith in sample 9b is around 50° anticlockwise with respect to the C plane of the dextral shear zone, and so the S planes at about 46° with respect to the C plane are nearly parallel to the original mylonitic foliation. Accordingly, shear strain, γ, was not estimated using θ_o in the WMZ.

Toward the shear zone, individual quartz grains, which show an elongate shape with strong undulose extinction, decrease in size progressively from 195 μm at sample 8a to 147 μm at sample 5a (Fig. 4) and form the matrix. Euhedral to subhedral feldspar grains decrease in size progressively, and become anhedral and rounded gradually forming porphyroclasts toward the shear zone. Biotite (4.1–6.9 modal %; Fig. 4) occurs as oriented subhedral grains, occasionally forming mica fish (Fig. 6a) with undulose extinction, acicular flakes, and secondary aggregates (Fig. 6b). Biotite is partly altered to chlorite. Hornblende (~0.4 modal %; Fig. 4) is a minor mafic mineral. Toward the shear zone, θ_o gradually decreases from 46° to 22°, whereas θ_m gradually decreases from 44° to 24° (Fig. 4), and ϕ_m gradually decreases from 48° to 20° (Fig. 5). The frequency of mineral orientation subparallel (±10°) to the S_o ranges 17–27% (microscopic data in Fig. 4) and 14–15% (BSE image data in Fig. 5b), whereas that subparallel (±10°) to the C′ ranges 7–12% (microscopic data in Fig. 4) and 10–13% (BSE image data in Fig. 5b) even though the shear bands are rarely observed in the WMZ under the microscope.

4.2. Moderately mylonitized zone (MMZ): characteristics of samples 4 and 3

Samples 4 and 3 have composite foliations S–C(–C′) defined by the orientation of elongate quartz aggregates, and aggregates of biotite ± hornblende. Each recrystallized quartz grain has elongate shape fabric oblique to S. The grain size of recrystallized quartz decreases down to 100 μm within the MMZ (Fig. 4). Feldspar grains are subhedral and porphyroclastic with undulose extinction. Biotite content slightly increases (7.1–7.5 modal %; Fig. 4) from the WMZ to MMZ. It occurs as oriented subhedral grains with undulose extinction. Secondary (recrystallized) biotite flakes also form aggregates defining the S foliation. Porphyroclastic feldspars are surrounded by matrix minerals including biotite flakes forming asymmetric tails (Fig. 6d). Hornblende is a minor mafic mineral (0.4–0.8 modal %; Fig. 4) and its elongation fabric defines S together with biotite flakes. Toward the shear zone, θ_o decreases from 16° to 12° (i.e. from $\gamma = 3.4$ to 4.7), whereas θ_m decreases from 17° to 13° (Fig. 4), and ϕ_m decreases from 4.5° to 1.5° (Fig. 5a). In samples 4a and 3a, the orientation of biotite and hornblende parallel to the S foliation is 24–26%. The portion of the grains that are parallel to the C plane is 22–23%, which is a gradual increase from sample 9a to 3a. In addition, the orientation parallel to the C′ plane presents about 15–18% increase from those in the WMZ (5–11%) (Fig. 4). The angle ϕ is less than θ especially in sample 3a, because of the feature in a sampling artifact. S and C′ in BSE images usually appear in combined forms, so the brighter areas of S and C′ often merge in binary BSE images. Such combined fabrics are counted as one domain. Consequently, the angles measured by Scion Image yield an orientation between S and C′, and thus the angle ϕ_m is less than θ_m.

4.3. Strongly mylonitized zone (SMZ): characteristics of samples 2 and 1

Fine-grained biotite–feldspar–quartz aggregate layers are strongly developed parallel to S and C (Fig. 6e). The number of layers increases toward the center of the shear zone. Small-scale C′ planes are pervasively developed within the layers (Fig. 6f). The grain size of recrystallized quartz in samples 2a and 1a continues inward decreasing to 67 μm (Fig. 4), which is finer than in the MSZ. Quartz aggregates show strongly elongate shapes commonly parallel to S and each quartz grain has strong undulose extinction. Feldspar grains occur as porphyroclasts and also as a fine-grained matrix aggregate. Most biotite flakes are very fine-grained and are anticlockwise oblique to S (Fig. 6e,f). A few larger subhedral biotite flakes occur with undulose extinction. Hornblende grains are rare. In the SMZ, the angle of θ_o is 13–15°, which is larger than sample 3a,

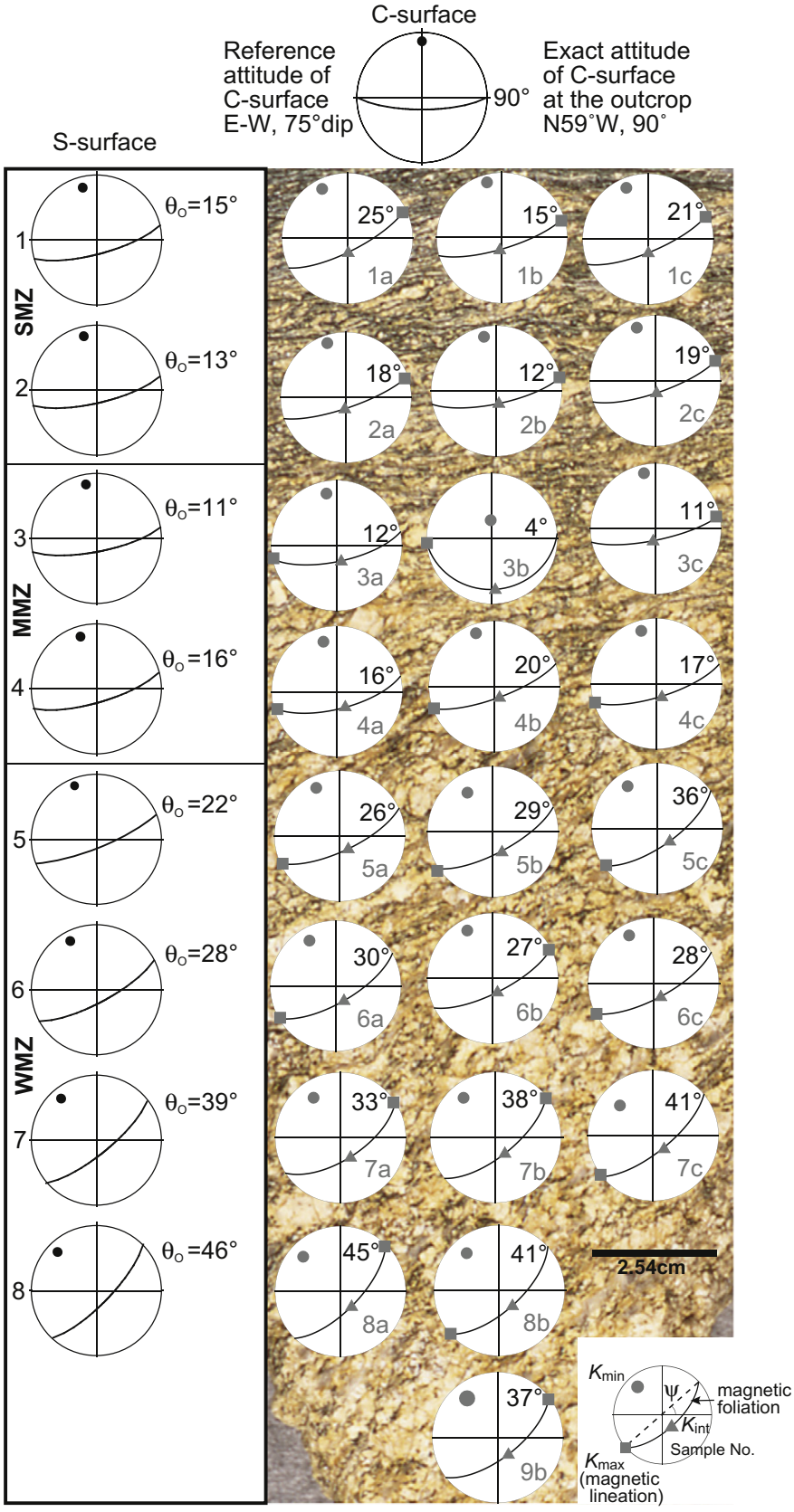

Fig. 7. Equal area, lower hemisphere projections of AMS orientation data. ψ is the angle between the strike of the K_{max}–K_{int} plane and of C, approximate to the angle between K_{max} and C.

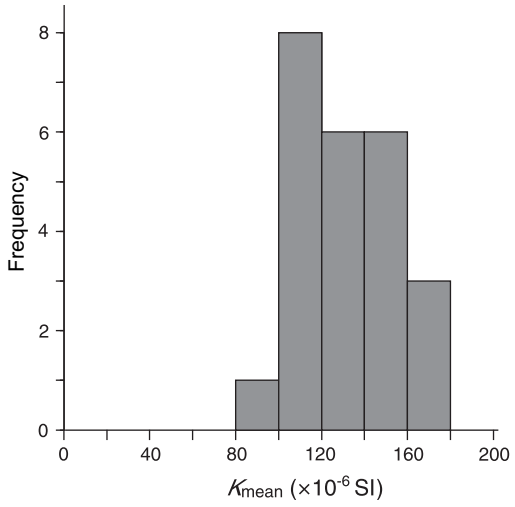

Fig. 8. Frequency histogram for bulk mean susceptibility K_{mean}.

and also increases from 5° to 15° toward the center of the shear zone (Fig. 4).

5. Magnetic analysis

AMS was measured at room temperature on a KLY-3S Spinner Kappabridge (Agico, Inc., Brno, Czech Republic) at the Department of Earth Science, Waseda University (Table 1). Magnetic susceptibilities were measured four times and the arithmetic mean and the standard deviation of the data were calculated. Equal area, lower hemisphere projections of K_{max}, K_{int} and K_{min} are illustrated in Fig. 7. The inclinations of K_{max} in all samples are nearly horizontal (0.0–6.4°: Table 1), therefore the angle between the strike of the K_{max}–K_{int} plane and of C approximates to the angle between K_{max} and C, and is labeled as ψ (Fig. 7).

As AMS is controlled by the sum of the contribution of each magnetic (diamagnetic, paramagnetic, ferromagnetic) mineral type in proportion to its volume fraction, characterizing the magnetic minerals in a sample is necessary. Diamagnetic minerals such as quartz and feldspar, which have weak and opposite susceptibility to the applied field have negligible effect in practice. Although high susceptible ferromagnetic minerals mask the paramagnetic contribution to AMS, our bulk mean susceptibility ($K_{mean} = (K_{max} + K_{int} + K_{min})/3$ (SI unit)) ranges from 98.8 to 173.8 × 10^{-6} (SI), consistent with the paramagnetic mineral control of AMS (Hrouda and Jelinek, 1990; Tarling and Hrouda, 1993). The histogram of K_{mean} measured for 24 core samples also shows a unimodal pattern (Fig. 8) consistent with paramagnetic minerals controlling AMS in the analyzed sample (Gleizes et al., 1993). An acquisition test of anhysteretic remnant magnetization (ARM) was used to determine if ferromagnetic minerals contributed to the AMS. Because ARM is only acquired by remanence-carrier minerals, such as ferromagnetic magnetite, the intensity of ARM acquisition is proportional to the volume fraction of ferromagnetic minerals (Jackson, 1991; Dunlop and Özdemir, 1997; Usui et al., 2006). Laboratory-induced ARM was acquired with an AF demagnetizer (Natsuhara-Giken DEM95) in a peak alternating-field (AF) of 120 mA and a bias field of 100 μT on samples 1c–7c. The calculated volume fraction of ferromagnetic magnetite in a sample from ARM intensities yields typical results of 10^{-6} volume % of magnetite, implying negligible magnetite contribution to the AMS (Table 2). Therefore paramagnetic minerals control the AMS and are dominated by biotite plus hornblende.

Table 2
ARM data and approximate volume percentage of magnetite calculated.

Sample	(ARM) sample (mA/m)[a]	Volume fraction of magnetite
1c	0.9	2.25 × 10^{-6}
2c	0.6	1.50 × 10^{-6}
3c	0.0	0.00 × 10^{-6}
4c	0.2	0.50 × 10^{-6}
5c	0.3	0.75 × 10^{-6}
6c	0.4	1.00 × 10^{-6}
7c	0.8	2.00 × 10^{-6}

[a] (ARM)sample ÷ (ARM)magnetite [=400 × 10^{3} (mA/m)]. Vol. % of magnetite = vol. fraction of magnetite × 100.

Such paramagnetic silicates can be directly related to the symmetry of the crystallographic lattice (Nye, 1985). As noted in Borradaile and Jackson (2004), only one AMS axis is parallel to the crystallographic *b*-axis for monoclinic minerals such as biotite and hornblende. In addition, K_{min} of mica is nearly parallel to the *c*-axis, i.e., the magnetic foliation, defined as the plane nearly normal to K_{min}, and statistically lies in the mica basal plane (Zapletal, 1990). K_{max} of amphibole is nearly parallel to the long dimension of the

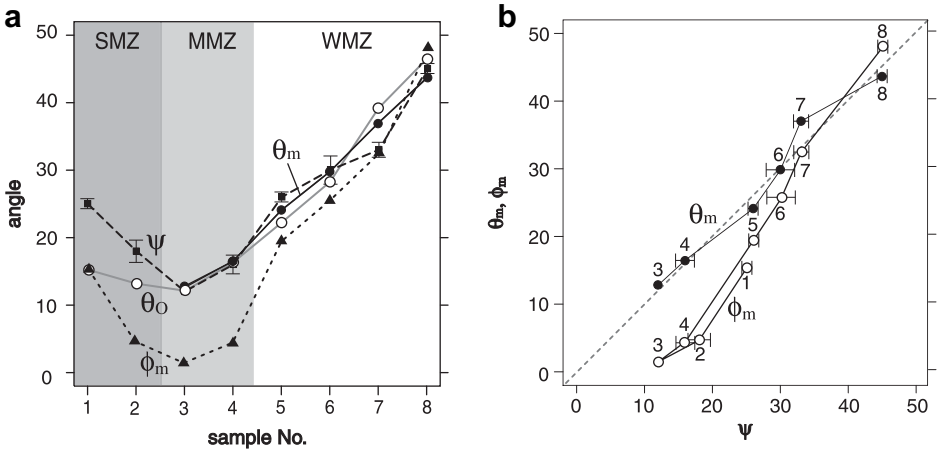

Fig. 9. (a) Variation in angles θ_o (observed S orientation), θ_m (mean vector for orientation of biotite + hornblende measured under the microscope), ϕ_m (mean vector for orientation of biotite + hornblende measured from the BSE image) and ψ (K_{max} direction) with respect to C across the shear zone from samples 8 to 1 (shear zone center). WMZ, MMZ and SMZ indicates weakly, moderately and strongly mylonitized zones, respectively. (b) Correlations of the angles between θ_m and ϕ_m with respect to j.

crystal, i.e., it is and will be parallel to a prominent amphibole lineation, if present (Pearce and Fueten, 1989). The P_j ranges from 1.057 to 1.119, and the T ranges from 0.30 to 0.55 except sample 3b, suggesting most samples have an oblate AMS ellipsoid (Table 1).

The AMS results (Fig. 7) lack evidence of inverse magnetic fabrics where K_{max} is the pole to the foliation of the rocks (Rochette et al., 1994) being a composite magnetic fabric where K_{max} is parallel to the intersection of two planar fabrics (e.g., Borradaile, 1988; Housen et al., 1993). Our results are similar to those of Aranguren et al. (1996), where the magnetic foliation, defined as the plane normal to K_{min}, lies between the S and C planes. In the WMZ (samples 9 to 5), ψ is 26–45°, decreasing toward the shear zone. In the MMZ (samples 4 to 3), ψ is 11–20°, decreasing toward the shear zone center. In the SMZ (samples 2 to 1), ψ is 12–25°, increasing toward the shear zone. The inclination of K_{int} for all samples except for sample 3b is fairly constant, ranging from 63° to 76°, and coincides with the dip angle (~75°) of the sample plane (Fig. 2). The magnetic foliation of sample 3b has a distinct difference from the others presumably because of the presence of large porphyroclasts within it deflecting grains defining the foliation, therefore the data from sample 3b are not included in the following interpretations.

6. Discussion

S–C mylonite provides composite magnetic fabric, where the magnetic foliation was considered to be in between S and C, because of the additive effect of two planar structures (Aranguren et al., 1996). However, our results for a small-scale shear zone are more complex.

The orientation data (Fig. 9) show that toward the center of the shear zone, the angles (θ_o, θ_m, ϕ_m and ψ) gradually decrease until sample 3 where the angles show minimums, and then increase to the center of the shear zone, where the angles gradually increase, which is contrary to expectation. Although shear strain γ can be calculated from θ_o, the angle between the S and C planes (e.g. Ramsay and Graham, 1970), this method is not directly applicable in the SMZ (samples 2 and 1), because the occurrence of slip along C′ which is dominantly developed in the SMZ (Fig. 3) brought about the back rotation of microlithon increasing θ_o angles (cf. Lister and Snoke, 1984; Platt, 1984; Dennis and Secor, 1987; Takagi, 1992). It is also notable that even with the C′ planes, the AMS K_{max} orientation (ψ) in the SSZ also increases toward the shear zone center. This increase in ψ is similar to that of ϕ_s, whereas that for θ_o is more gentle (see Fig. 9a). Such difference in the inclination between ϕ_s and θ_o is probably because the SPO of very fine-grained biotite flakes in the SMZ tends to be anticlockwise to the trace of mesoscopic S foliation. This geometry is well documented in sample 1a where the angle for 20–40° with respect to C has considerable peaks larger than the peak of C′ in Fig. 5. Therefore, the abrupt increase in ψ in samples 2 and 1 is interpreted to result from individual fine-grained biotite flakes in the matrix of mylonite that is oblique (anticlockwise) to S (Fig. 6e,f). As a result even though some amount of parallel biotite flakes are developed in the SMZ along the C′ planes, the mean orientation of biotite flakes or even biotite aggregates (bright domain in BSE image) is greater than θ_o for the observed orientation of S.

In samples 8 to 5 (WMZ) where S plane dominates, the AMS orientation ψ almost corresponds to θ_m and θ_o, and is a little larger than ϕ_m (measured from BSE images) (Fig. 9). In samples 4 and 3 (MMZ) where S–C fabric is present, ψ almost corresponds to θ_m and θ_o as well as in WMZ, but does not correspond to ϕ_m. The angle ϕ_m is smaller than θ_m because of the measurement characteristics of the BSE images recording the bright domain that are aggregates of biotite (+hornblende). In samples 2 and 1 where the C′ plane is dominantly developed, the angle ϕ_m is smaller than θ_m for the same reason as in MMZ.

In summary, the K_{max} orientation ψ coincides with the mean vector of the preferred orientation of individual biotite (+hornblende) grains, but does not coincide well with the mean vector of the preferred orientation of the bright domain given the aggregate rather than the individual grain geometry is composed of biotite (+hornblende). This coincidence supports the interpretation that the magnetic fabric reflects contributions from the anisotropy of the SPO of paramagnetic biotite.

Acknowledgements

We thank Dr N. Nakamura (Tohoku University), for his valuable comments and for providing the magnetic equipment. Thanks are also due to Dr K. Shimada (JAEA) for fruitful comments and to Dr T.J. Fagan (Waseda University) for correcting the English. We also thank Dr I. Iwasaki, Mr K. Suzuki and Mr K. Yonemochi (Waseda University) for their advice on sample preparation during this work. Statistical operations were performed with the R statistical environment developed by R Development Core Team (http://www.r-project.org/) and the package 'circular' by Ulric Lund and Claudio Agostinelli. We are also grateful to Prof. W.M. Dunne (Editor), Dr G.J. Borradaile and an anonymous reviewer for constructive comments and correcting the English.

References

Aranguren, A., Cuevas, J., Tubia, J.M., 1996. Composite magnetic fabrics from S–C mylonites. Journal of Structural Geology 18, 863–869.
Archanjo, C.J., Bouchez, J.L., Corsini, M., Vauchez, A., 1994. The Pombal granite pluton: magnetic fabric, emplacement and relationships with the Brasiliano strike-slip setting of NE Brazil (Paraiba State). Journal of Structural Geology 16, 323–335.
Arita, M., 1988. Petrographical studies on granitic rocks in the Kojima Peninsula and Shiwaku Islands, the central parts of Seto Island sea, southwest Japan: petrogenetic and magmatogenetic origin of granitic rocks. Journal of the Geological Society of Japan 94, 279–293.
Borradaile, G.J., 1988. Magnetic susceptibility, petrofabrics and strain. Tectonophysics 156, 1–20.
Borradaile, G.J., Henry, B., 1997. Tectonic applications of magnetic susceptibility and its anisotropy. Earth-Science Reviews 42, 49–93.
Borradaile, G.J., Jackson, M., 2004. Anisotropy of magnetic susceptibility (AMS): magnetic petrofabrics of deformed rocks. In: Martin-Hernandez (Ed.), Magnetic Fabric-Methods and Applications. Geological Society, Special Publications vol. 238, pp. 299–360.
Borradaile, G.J., Tarling, D.H., 1981. The influence of deformation mechanisms on magnetic fabrics in weakly deformed rocks. Tectonophysics 77, 151–168.
Dennis, A.J., Secor, D.T., 1987. A model for the development of crenulations in shear zones with applications from the Southern Appalachian Piedmont. Journal of Structural Geology 7, 809–817.
Dunlop, D., Özdemir, Ö., 1997. Rock Magnetism: Fundamental and Frontiers. Cambridge University Press, Cambridge, 573 pp.
Gleizes, G., Nédélec, A., Bouchez, J.-L., Autran, A., Rochette, P., 1993. Magnetic susceptibility of the Mont-Louis Andorra ilmenite-type granite (Pyrenees): a new tool for the petrographic characterization and regional mapping of zoned granite plutons. Journal of Geophysical Research 98 (B3), 4317–4331.
Housen, B.A., Richter, C., van der Pluijm, B.A., 1993. Composite magnetic anisotropy fabrics: experiments, numerical models, and implications for the quantification of rock fabrics. Tectonophysics 220, 1–12.
Hrouda, F., 1982. Magnetic anisotropy of rocks and its application in geology and geophysics. Geophysical Surveys 5, 37–82.
Hrouda, F., Jelinek, V., 1990. Resolution of ferromagnetic and paramagnetic anisotropies in rocks, using combined low-field and high-field measurements. Geophysical Journal International 103, 75–84.
Ishihara, S., 1981. The Granitoid Series and Mineralization. Economic Geology 75th Annual Volume, pp. 458–484.
Jackson, M., 1991. Anisotropy of magnetic remanence: a brief review of mineralogical sources, physical origins, and geological applications, and comparison with susceptibility anisotropy. Pure and Applied Geophysics 136, 1–28.
Jammalamadaka, S.R., SenGupta, A. (Eds.), 2001. Topics in Circular Statistics. World Scientific, Singapore, 322 pp.
Jelinek, V., 1981. Characterization of the magnetic fabric of rocks. Tectonophysics 79, T63–T67.
Lister, G.S., Snoke, A.W., 1984. S–C mylonites. Journal of Structural Geology 6, 617–638.

Michibayashi, K., Murakami, M., 2007. Development of a shear band cleavage as a result of strain partitioning. Journal of Structural Geology 29, 1070–1082.
Nye, J.F., 1985. Physical Properties of Crystals. Oxford University Press, New York, 329 pp.
Pearce, G.W., Fueten, F., 1989. An intensive study of magnetic susceptibility anisotropy of amphibolite layers of the Thompson Belt, North Manitoba. Tectonophysics 162, 315–329.
Platt, J.P., 1984. Secondary cleavages in ductile shear zones. Journal of Structural Geology 6, 439–442.
Ramsay, J.G., Graham, R.H., 1970. Strain variation in shear belts. Canadian Journal of Earth Sciences 7, 786–813.
Rochette, P., 1987. Magnetic susceptibility of the rock matrix related to magnetic fabric studies. Journal of Structural Geology 9, 1015–1020.
Rochette, P., Scaillet, B., Guillot, S., Le Fort, P., Pecher, A., 1994. Magnetic properties of the High Himalayan leucogranites: structural implications. Earth and Planetary Science Letters 126, 217–234.
Stephens, 1970. Use of the Kolmogorov–Smironov, Cramer–Von Mises and related statistics without extensive tables. Journal of the Royal Statistical Society. Series B (Methodological) 32, 115–122.
Takagi, H., 1992. Development of composite planar fabric in mylonites along the Median Tectonic Line, southwest Japan. The Island Arc 1, 92–102.
Tarling, D.H., Hrouda, F., 1993. The Magnetic Anisotropy of Rocks. Chapman and Hall, London, 217 pp.
Tomezzoli, R.N., MacDonald, W.D., Tickyj, H., 2003. Composite magnetic fabrics and S–C structure in granitic gneiss of Cerro de los Viejos, La Pampa province, Argentina. Journal of Structural Geology 25, 159–169.
Usui, Y., Nakamura, N., Yoshida, T., 2006. Magnetite microexsolutions in silicate and magmatic flow fabric of the Goyozan granitoid (NE Japan): significance of partial remanence anisotropy. Journal of Geophysical Research 111, B11101. doi:10.1029/2005JB004183.
Zapletal, K., 1990. Low-field susceptibility anisotropy of some biotite crystals. Physics of the Earth and Planetary Interiors 63, 85–97.